CrossMark

RESEARCH PAPER

Improved photocatalytic degradation of Orange G using hybrid nanofibers

**Mpho Ledwaba · Nkosiphile Masilela ·
Tebello Nyokong · Edith Antunes**

Abstract Functionalised electrospun polyamide-6 (PA-6) nanofibres incorporating gadolinium oxide nanoparticles conjugated to zinc tetracarboxyphenoxy phthalocyanine (ZnTCPPc) as the sensitizer were prepared for the photocatalytic degradation of Orange G. Fibres incorporating the phthalocyanine alone or a mixture of the nanoparticles and phthalocyanine were also generated. The singlet oxygen-generating ability of the sensitizer was shown to be maintained within the fibre mat, with the singlet oxygen quantum yields increasing upon incorporation of the magnetic nanoparticles. Consequently, the rate of the photodegradation of Orange G was observed to increase with an increase in singlet oxygen quantum yield. A reduction in the half-lives for the functionalised nanofibres was recorded in the presence of the magnetic nanoparticles, indicating an improvement in the efficiency of the degradation process.

M. Ledwaba · N. Masilela · T. Nyokong · E. Antunes (✉)
Department of Chemistry, Rhodes University,
Grahamstown 6140, South Africa
e-mail: ebeukes@uwc.ac.za

E. Antunes
Department of Chemistry, University of the Western Cape,
Bellville 7535, South Africa

Introduction

The highly conjugated, planar metallo-phthalocyanines (MPcs) with their 18-π electron system absorb intensely in the red region of the visible spectrum, where variation in the central metal and the type, number and position of substituents attached to the macrocycle have a great influence on the chemical properties of the MPc (Rosenthal and Ben Hur 1996; Kadish et al. 2003). This ability to tailor the phthalocyanines for specific purposes allows them to be applied in a diverse range of fields including electrocatalysis (Agboola et al. 2006; Nyokong 2006), as sensors (Nyokong 2006), photosensitizers in photodynamic therapy (PDT) (Okura 2001) and photocatalysis (Wöhrle et al. 2004). The Pc's high thermal and photo-stability, excellent absorption of visible light, chemical inertness and the MPc's proficiency in producing singlet oxygen from ground state molecular oxygen in the presence of light are well documented (Agboola et al. 2006; Okura 2001; Wöhrle et al. 2004; Marais et al. 2007; Ali and van Lier 1999), making the Pcs especially promising as photocatalysts. Phthalocyanines have been employed as both heterogenous and homogenous catalysts, both in solution or on solid support systems such as resins (such as amberlite) (Marais et al. 2007) and electrospun nanofibres (Zugle et al. 2011, 2012; Mosinger et al. 2009; Tombe et al. 2012. Lang et al. 2016). Immobilisation onto solid support systems is particularly attractive since the possibility of catalyst recycling becomes plausible (Lang et al. 2016). Electrospinning is a promising technique, since molecules with a variety of functional purposes may be easily incorporated and the technique itself is convenient,

simple, cheap and reproducible and the fibres produced possess large surface areas, high porosity, mechanical strength and flexibility.

Magnetic nanoparticles have found application in numerous fields including the biomedical fields such as drug delivery (Chomoucka et al. 2010), magnetic resonance imaging (MRI) (Mornet et al. 2006), hyperthermia therapy (Bin Na et al. 2009), as well as environmental remediation (Elliott and Zhang 2001). Additionally, the nanoparticle surface allows tailoring of the NP for specific purposes upon functionalisation (Deng et al. 2005). Incorporation of magnetic nanoparticles (MNPs) with phthalocyanines (either by simple mixing or conjugation to the Pc) has consistently shown an increase in the triplet quantum yield and therefore the singlet oxygen-generating ability (measured as singlet oxygen quantum yields) of the phthalocyanine (Ledwaba et al. 2015; Modisha et al. 2013a; Idowu and Nyokong 2012). The increase in the triplet quantum yield is likely to be due to the enhanced intersystem crossing of the excited Pc due to the heavy metal atom effect (Modisha et al. 2013b).

The widespread use of organic dyes, especially azo dyes such as Orange G (OG), in industrial wastewater is a serious environmental issue since they are considered toxic (Stylidi et al. 2004). Various physicochemical and biological methods such as filtration, coagulation, precipitation, adsorption, ion exchange and oxidation techniques have been employed for removal of the dye from wastewater (Aplin and Wait 2000; Neppolian et al. 2002; Sun et al. 2006). However, the cost and low efficiency of these techniques have precluded their use. Phthalocyanines have been successfully employed in the photodegradation of the dye to less harmful by-products through the use of light and the singlet oxygen generated by the Pc (Aplin and Wait 2000; Neppolian et al. 2002; Sun et al. 2006), offering a promising alternative.

Owing to the efficient photocatalytic degradation of OG previously reported by our group using a zinc tetracarboxyphenoxy phthalocyanine (ZnTCPPc) conjugated to Gd_2O_3 nanoparticles (MNPs) (Ledwaba et al. 2015), we report on the immobilisation of this conjugate (Fig. 1) in a polyamide-6 (PA-6) electrospun fibre. The functionalised fibres were subsequently employed for the photodegradation of Orange G, where the fibre is simply suspended in a solution. The results obtained were related to those where the conjugates were not embedded in the fibre. Although several studies (Sun et al. 2006; Tombe et al. 2013) have reported on
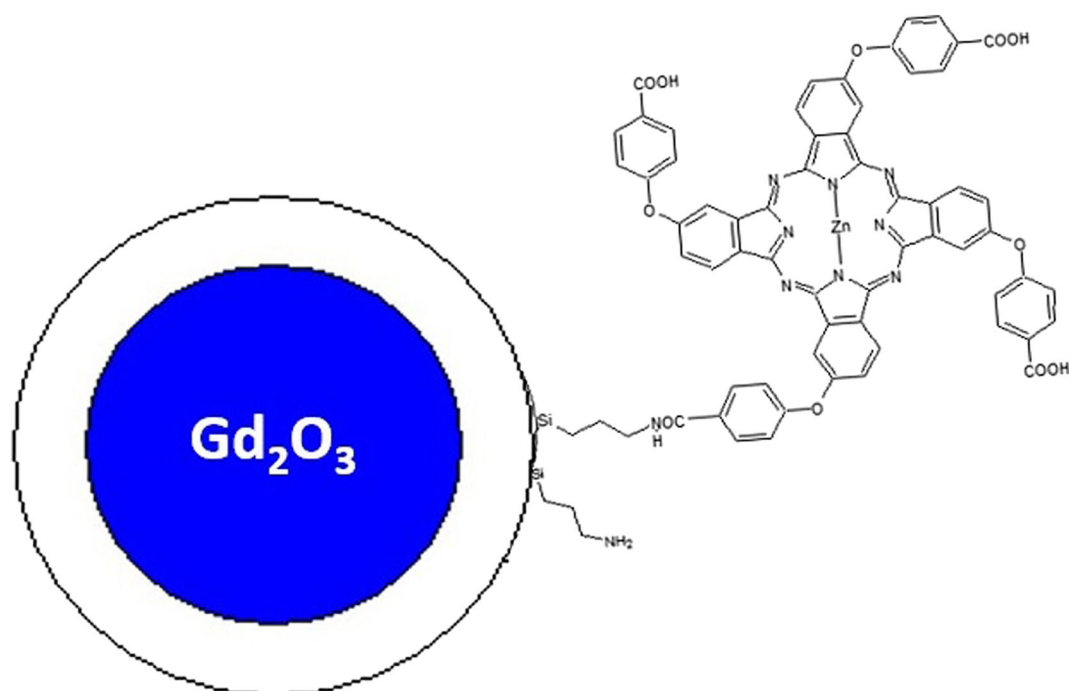

Fig. 1 Proposed structure for the ZnTCPPc-MNP (conjugate)

the photodegradation of OG, incorporation of the ZnTCPPc-Gd$_2$O$_3$ NP conjugate embedded in a polyamide electrospun fibre for the photodegradation of OG has not been reported.

Experimental

Materials

PA-6 Ultramide® B grades (i.e. B24, B27, B32 and B36) were supplied by BASF or Sigma-Aldrich. The average molecular weights (g/mol) of the polymers were 70,000, 80,000, 90,000 and 100,000 for B24, B27, B32 and B36, respectively. Anthracene-9,10-bismethyl malonate (ADMA), acetic acid (98%), formic acid (99.8%), dimethyl sulfoxide (DMSO) and OG were purchased from Sigma-Aldrich. Water collected from a Milli-Q water purification system (Millipore Corp., Bedford, MA, USA) was used for the preparation of all aqueous solutions. The amino-functionalised gadolinium oxide nanoparticles (MNPs) (Ledwaba et al. 2015), ZnTCPPc (Li et al. 2008) and the ZnTCPPc-MNP conjugates (Ledwaba et al. 2015) were synthesised according to methods documented previously in the literature. The samples are referred to as ZnTCPPc-MNP (conj) for the conjugate between the Pc and MNP and as ZnTCPPc-MNP (mix) for a simple mixture of the Pc and MNP.

Equipment

A scanning electron microscope (JEOL JSM 840 scanning electron microscope (SEM)) operating at an accelerating voltage of 20 kV was used to examine the morphology of the electrospun nanofibres. Using the Cell D software from Olympus, the average fibre diameter together with the standard deviations was determined from 70 measurements. An INCA PENTA FET coupled to a VAGA TESCAM operating at a 20-kV accelerating voltage was used to collect the energy-dispersive X-ray spectroscopy (EDX) data. UV-Vis absorption spectra were measured at room temperature on a Shimadzu UV-2550 spectrophotometer using a 1-cm path length cuvette for the solution studies.

A 300-W halogen lamp together with 600 nm glass (Schott) and water filters (which were used to filter off ultraviolet and far infrared radiation, respectively) was used to determine the singlet oxygen quantum yields.

An additional filter, an interference filter (Intor, 670 nm with a bandwidth of 40 nm), was positioned in the light path before the reaction system. Using a power meter (POWER MAX 5100 Molectron Detector Inc.), the light intensity reaching the reaction setup was found to be 1.3×10^{19} photons cm^{-2} s^{-1}. The photolysis setup was also used to carry out the photodegradation experiments; however, the intensity of the light reaching the reaction holder for these photodegradation studies was higher, at 3.2×10^{20} photons cm^{-2} s^{-1}.

Electrospinning methods

Identical procedures were followed for all four polymer grades (i.e. PA-6 grades B24, B27, B32 and B36) to obtain the electrospun fibres. The PA-6 pellets were dissolved in formic acid and acetic acid in a 1:1 ratio to give a 14 wt% solution and stirred for 24 h at room temperature. The unfunctionalised electrospun fibres for each of the grades were then prepared using a 5-mL syringe fitted with a hypodermic needle (inner diameter of 0.1 mm) at a flow rate of 0.2 mL h^{-1} to give the fibre mats. The solutions were electrospun at 30 kV onto a grounded collector covered with foil where the solidified nanofibres were collected at ambient temperature and 25% humidity. The full characterisation of these electrospun fibres is given in the supporting information. The functionalised fibre mats were prepared as follows: the samples (a) ZnTCPPc (2 mg), (b) ZnTCPPc-MNP (conj) (3 mg) or (c) ZnTCPPc/MNP (mix) (3 mg) were added to the polymer solution (14 wt%, B32 grade) in formic acid and acetic acid (1:1 ratio) and stirred overnight. The functionalised electrospun fibres were then prepared using the same parameters as before to give the (a) PA/ZnTCPPc, (b) PA/ZnTCPPc-MNP (conj) and (c) PA/ZnTCPPc-MNP (mix) fibre mats. These fibre mats were immersed in the Orange G solution for 30 min prior to the photocatalytic experiments being carried out.

Results and discussion

Characterisation of the ZnTCPPc-MNP conjugate

The characterisation of the ZnTCPPc-MNP conjugate itself has been previously described (Ledwaba et al. 2015). Analysis of the TEM data revealed the silica-coated Gd$_2$O$_3$ NPs to be approximately 15 nm in

size, with the size increasing slightly to 17 nm upon conjugation to the ZnTCPPc. The TEM images also revealed a change in appearance of the sample upon conjugation and that the nanocomposite is still well dispersed and uniform in size (Ledwaba et al. 2015), unlike the Fe_3O_4 NP conjugates obtained by Modisha et al. where the samples remained highly aggregated (Modisha et al. 2013a, b). The information derived from the XRD powder diffraction patterns for the Gd_2O_3 NP conjugates was not useful as significant line broadening is typically observed with Gd_2O_3 NPs smaller than 20 nm (Zhou et al. 2012). The UV-Vis spectra of ZnTCPPc in DMSO (Fig. 2) reveal the presence of the Q and B bands in DMSO, which do not shift upon formation of the conjugate with the MNP or with a simple mixture of the ZnTCPPc and the MNP, although an increase in the B band at ~360 nm due to the MNP is observed. The ground state electronic spectra of the samples show monomeric behaviour as evidenced by the single narrow Q band (Idowu and Nyokong 2008), while the MNPs show a broad absorption peak (Fig. 2) (i) beginning at approximately 500 nm, and thus, this increase in absorption for the Pc conjugate (Fig. 2) (iii) and mix (Fig. 2) (iv) samples is attributed to the presence of the MNP.

Characterisation of the electrospun fibres

Scanning electron microscopy

The fibre diameter and morphology of the electrospun nanofibres were assessed using SEM. The average
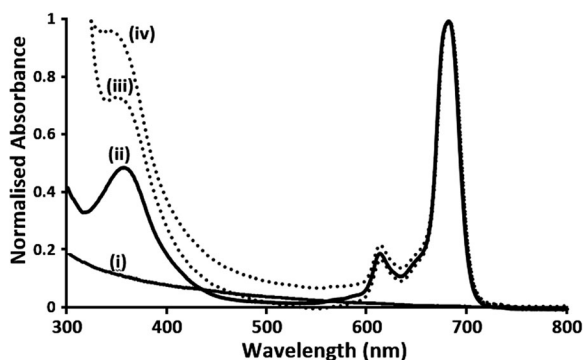

Fig. 2 Normalised UV-Vis absorption spectra in DMSO of (*i*) the MNPs, (*ii*) ZnTCPPc, (*iii*) ZnTCPPc-MNP (conj) and (*iv*) ZnTCPPc-MNP (mix) at a concentration of ~10^{-6} M

diameter of the fibres for each sample including the polyamide polymer (PA) alone (for each of the four grades B24, B27, B32 and B37) and the fibres functionalised with ZnTCPPc, ZnTCPPc-MNP (conj) and ZnTCPPc-MNP (mix) were determined using the Cell D software from Olympus following imaging. Prior to functionalisation, various polymer concentrations were used to optimize fibre formation, with the SEM images revealing fibres that possessed junctions and bundles at lower polymer concentrations, indicating that the fibres were still wet when reaching the collection plate. By increasing the solution viscosity (i.e. increasing the polymer concentration), uniform, continuous single fibres with few beads and junctions were obtained. As observed in the SEM images, the fibre surfaces were defect free and possessed consistent fibre diameters (Fig. S1, ESI). The best fibres obtained under the conditions used were the PA B32 fibres (Fig. S2 and Table S2, ESI), and the functionalised fibres were thus produced using the B32 grade polyamide pellets (as outlined in the experimental "Electrospinning methods" section). The full characterisation of these fibres is detailed in the supplementary information.

The SEM images obtained for the functionalised and the unfunctionalised polyamide fibres revealed wholly uniform fibres that were defect free (i.e. no beads were present or formed), with controllable diameters (Fig. 3). The fibre diameters ranged from 200 to 1050 nm in size.

The PA/ZnTCPPc-MNP (conj) fibre (Fig. 3b) shows a slight increase in fibre diameter as compared to the Pc alone (PA/ZnTCPPc, Fig. 3a), which may be expected considering the additional presence of the MNPs in the former sample. The conjugate is bulkier compared to the Pc alone, and it is expected to increase the overall viscosity of the polymer solution. Analysis of the SEM images obtained for PA/ZnTCPPc-MNP (mix) revealed a further increase; however, these fibres also showed the presence of several beads (Fig. 3c), implying that the fibres were of lower quality.

Energy dispersive X-ray spectroscopy

The chemical composition of the fibres produced as revealed by the EDX data was expected to indicate whether the ZnTCPPc and the MNPs were successfully incorporated into the fibre matrix. The EDX spectra of the fibres (Fig. 4) confirm the presence of the MNPs as shown by the presence of Gd in the spectra in Fig. 4a–d. Interestingly, Fig. 4d also reveals the presence of smaller

Fig. 3 SEM images of the functionalised nanofibre mats of **a** PA/ZnTCPPc, **b** PA/ZnTCPPc-MNPs (conj) and **c** PA/ZnTCPPc-MNP (mix)
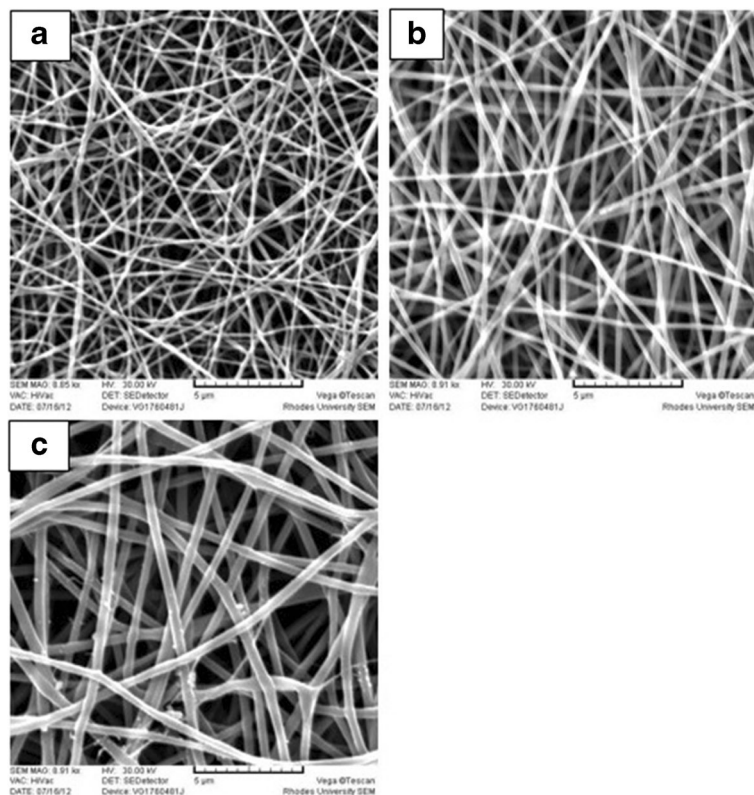
amounts of Gd in the PA/ZnTCPPc-MNP (mix) sample. Figure 4b shows the spectrum obtained for the fibre formed with the ZnTCPPc alone, revealing only C, N and O as expected for the Pc incorporated into a polyamide fibre but also Si, which may be an impurity obtained from glassware. Si and O are expected for the conjugate and mix samples, as the MNPs are encapsulated with a silica shell. The additional presence of trace amounts of Al may be accounted for by the aluminium foil that is used to collect the fibres during production of the fibres. Successful formation and incorporation of the ZnTCPPc-MNP conjugate and ZnTCPPc-MNP mix samples into the fibres are thus verified by the EDX data, as were previously confirmed by the UV-Vis spectra (Fig. 2).

Singlet oxygen-generating ability of the functionalised fibres

Singlet oxygen plays a significant role in photocatalytic reactions and it is therefore essential to determine whether the singlet oxygen-generating ability of the sensitizer (ZnTCPPc) alone, together with the ZnTCPPc conjugated to, or simply mixed with, the MNPs, is retained upon incorporation into a nanofibre mat. The ZnTCPPc-MNP (conj) and the ZnTCPPc-MNP (mix) samples alone (i.e. not incorporated into a nanofibre) were previously shown to have singlet oxygen quantum yields (Φ_Δ) of 0.36 and 0.49, respectively, as determined by use of the singlet oxygen chemical quencher diphenylisobenzofuran (DPBF) (Ledwaba et al. 2015). The sensitizer alone (i.e. ZnTCPPc) has been shown to be highly photo-stable (Achadu et al. 2016; Oluwole et al. 2016 and Ledwaba et al. 2015), making use of this phthalocyanine for the photodegradation of Orange G ideal. The higher the Φ_Δ, the greater the ability of the sensitizer to produce singlet oxygen, and photocatalytic reactions are therefore expected to be more efficient. The yields obtained for the conjugate and the mixture showed an improvement in the Φ_Δ obtained for the ZnTCPPc alone (0.32) upon introduction of the MNPs. Similar studies using Fe_3O_4 NPs with zinc octacarboxy phthalocyanine (ZnOCPc) by Modisha et al. (2013a, b) also revealed a marked improvement.
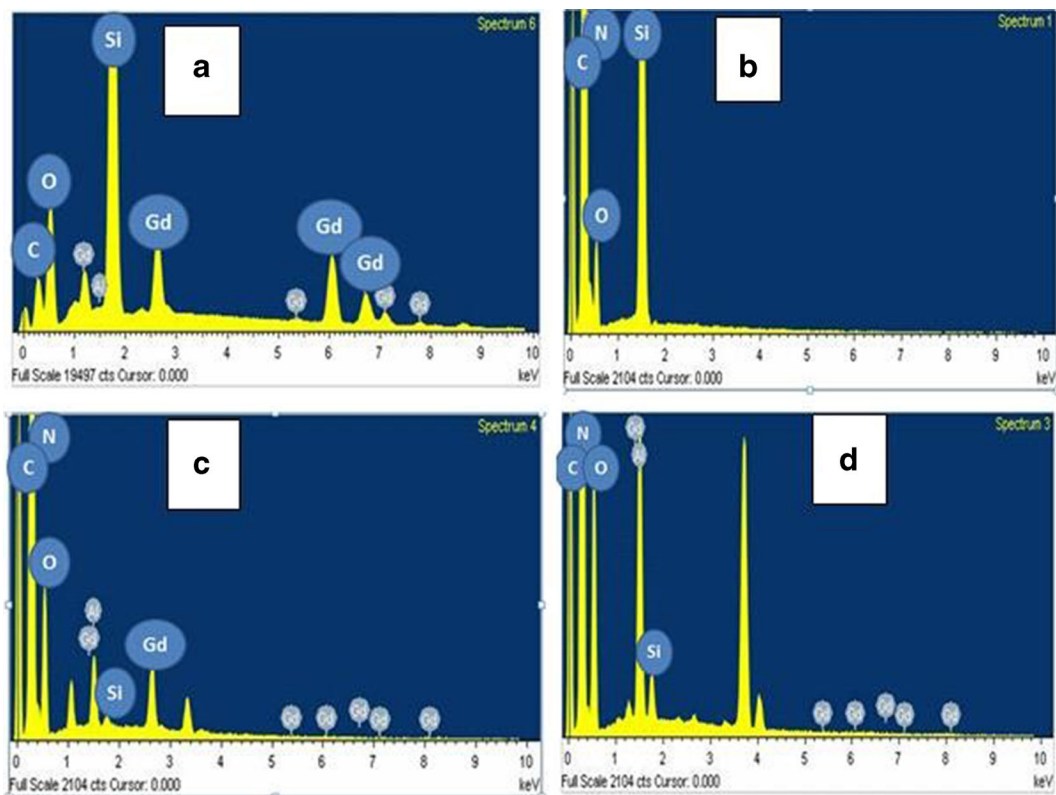
Fig. 4 EDX spectra of **a** PA/MNP (conj), **b** PA/ZnTCPPc, **c** PA/ZnTCPPc-MNP (conj) and **d** PA/ZnTCPPc-MNP (mix) nanofibre mats

The singlet oxygen-generating abilities of the various functionalised nanofibre mats were determined in an aqueous medium using ADMA as a chemical quencher, since ADMA is soluble in water. The lower singlet oxygen quantum yields observed in water in comparison to organic solvents is due to the lower solubility of oxygen in water. Thus, lower singlet oxygen quantum

yields are expected for analyses carried out in water (in contrast to studies using DPBF as the chemical quencher). Data obtained using ADMA is relevant to our studies since we are exploring the use of these nanofibre mats as a solid support for the sensitizer and sensitizer hybrids for the photocatalysis of Orange G, to less harmful by-products, which may be found in the dye

Fig. 5 The UV-Vis spectral changes observed following the photolysis of ADMA in an aqueous solution for 30 min with 15 mg of the PA/ZnTCPPc-MNP (conj) fibre suspended in solution. ADMA starting concentration is 3.9×10^{-5} mol dm^{-3}. Irradiation interval is 5 min
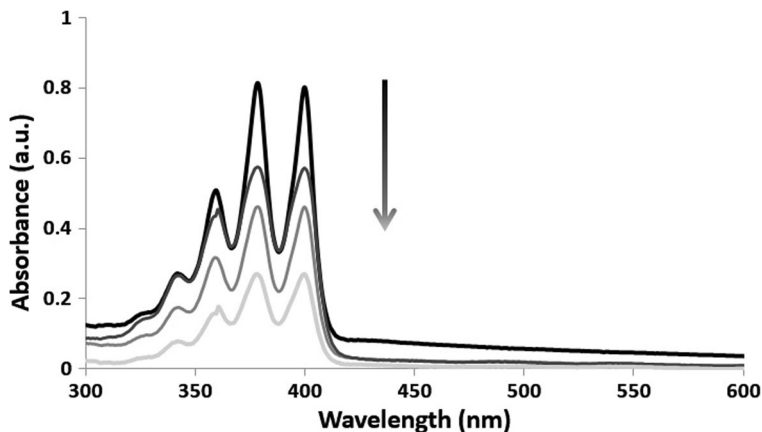
industry's waste water and the nanofibre mats were immersed in the Orange G solution for 30 min prior to the photocatalytic experiments being carried out. The singlet oxygen quantum yields (Φ_Δ) were thus determined for the ZnTCPPc and ZnTCPPc-MNP (conj) and ZnTCPPc-MNP (mix) incorporated into the various fibre mats in aqueous media by monitoring the photodegradation of ADMA at 380 nm (Fig. 5). Fifteen milligrams of the modified fibres (PA/ZnTCPPc, PA/ZnTCPPC-MNP (conj) and PA/ZnTCPPc-MNP (mix)) were suspended in an aqueous solution of ADMA and irradiated for 30 min at 60 W using the photolysis setup described in the experimental section. The quantum yields (Φ_{ADMA}) were calculated using Eq. (1) (Spiller et al. 1998), using the molar extinction coefficient of ADMA in water, $\log\varepsilon$ = 4.1 (Ogunsipe and Nyokong 2005):

$$(\phi_{ADMA}) = \frac{(C_O - C_t)V_B}{I_{abs} \cdot t} \qquad (1)$$

where C_o and C_t are the ADMA concentrations at the start and end of the irradiation period, respectively, V_B is the solution volume, t is the irradiation time and I_{abs} is defined by Eq. (2):

$$I_{abs} = \frac{\alpha \cdot A \cdot I}{N_A} \qquad (2)$$

where $a = 1 - 10^{-A(\lambda)}$, $A(\lambda)$ is the absorbance of the sensitizer at the irradiation wavelength, A is the irradiated area (2.5 cm^2) and I is the intensity of light (1.3 × 10^{19} photons cm^{-2} s^{-1}), while N_A is Avogadro's constant. The absorbance used for Eq. (2) is not the phthalocyanines in solution but the phthalocyanine embedded in the fibre which is placed on a glass slide. The light intensity measured refers to the light reaching the UV-Vis cuvette and it is expected that some of the light is scattered. Thus, the Φ_Δ values reported herein for the nanofibres are estimates. The singlet oxygen quantum yields were calculated using Eq. (3) (Foote 1979):

$$\frac{1}{\phi_{ADMA}} = \frac{1}{\phi_\Delta} + \frac{1}{\phi_\Delta} \cdot \frac{k_d}{k_a} \cdot \frac{1}{[ADMA]} \qquad (3)$$

where k_d is the decay constant of singlet oxygen and k_a is the rate constant for the reaction of ADMA with $^1O_2$ (that is $^1\Delta_g$). The intercept obtained from the plot of $1/\Phi_{ADMA}$ versus $1/[ADMA]$ reveals $1/\Phi_\Delta$.
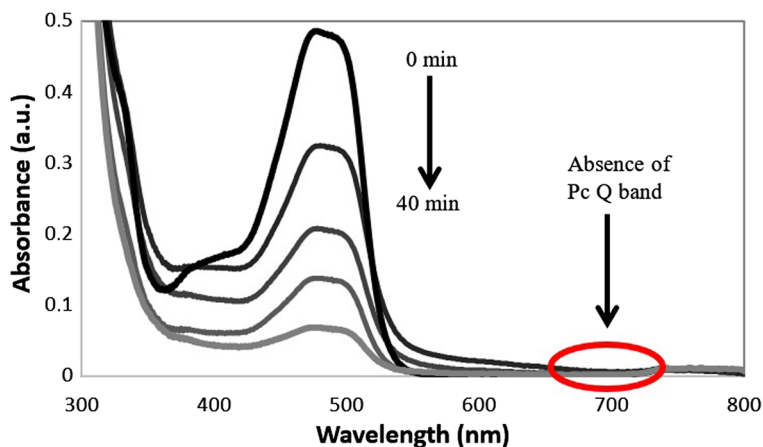
Table 1 Singlet oxygen quantum yields of the variously functionalised nanofibres

Sample	Fibre diameter (nm)	Φ_Δ (in water)
PA/ZnTCPPc	225	0.16
PA/ZnTCPPc-MNP (conj)	575	0.12
PA/ZnTCPPc-MNP (mix)	1025	0.21

The UV-Vis spectra show the distinctive bands associated with ADMA (Fig. 5) but not that of the Pc, indicating that the Pc is firmly embedded in the fibre and is not leaching out. As the photolysis proceeds, there is a decrease in the absorption intensity of the ADMA owing to the production of singlet oxygen by the phthalocyanine and the consequent degradation of the chemical quencher. The results, shown in Table 1, reveal that the phthalocyanine is indeed still capable of producing singlet oxygen when incorporated into a fibre and additionally when conjugated to, or simply mixed with, the MNPs. The Φ_Δ values of the Pc (0.16) are shown to decrease upon conjugation to the MNP (0.12), but these values increase when the Pc is simply mixed with the MNP (0.21) and embedded in the fibre. This may likely be due to the differing amounts of the phthalocyanine sensitizer actually present in each of the fibre mats. The different amounts may be due to the actual procedures used in synthesizing and purifying the conjugate, while the mix sample is simply prepared by adding the sensitizer to the NP (Ledwaba et al. 2015). It is possible therefore that the conjugate sample contains less of the phthalocyanine sensitizer than the mix sample, which accounts for the decrease observed in the singlet oxygen quantum yield. It is also possible that the polyamide fibre is responsible for the decrease in the singlet oxygen quantum yield since polyamides have a lower oxygen permeability in comparison to other fibres. However, Modisha and Nyokong (2014) and Goethals et al. (2014) both showed the successful incorporation of the phthalocyanine into the fibre without affecting the Pc's ability to produce singlet oxygen. This may be due to the greater amount of sensitizer present on the fibre surface. A similar trend was observed for the samples not embedded in a fibre matrix, i.e. the Φ_Δ obtained for the ZnTCPPc-MNP (mix) sample was 0.49, while the conjugate possessed lower Φ_Δ values at 0.36. These latter values

are higher, and it is expected for reactions carried out in organic solvents, since the solubility of oxygen in water is lower. Modisha et al. using Fe_3O_4 nanoparticles revealed similar results where the sensitizing ability of the Pc was retained and improved by the presence of the MNPs upon electrospinning (Modisha and Nyokong 2014). The PA/ZnTCPPc-MNP (mix)-functionalised fibre is therefore expected to be efficient in the photodegradation of Orange G. The singlet oxygen generated that reacts with the singlet oxygen trap is likely only taking place mostly on the surface of the fibre, since any singlet oxygen generated inside the fibre (where already the oxygen content would be lower) would have to diffuse to the surface of the fibre mat since the singlet oxygen trap is not likely to diffuse into the fibres. The values obtained for these fibres are thus surprising. However, several reports by our group have previously shown incorporation of the phthalocyanine sensitizer without serious deleterious effects on the singlet oxygen quantum yield, i.e. the singlet oxygen-generating abilities of the sensitizer remained intact (Zugle et al. 2011, Tombe et al. 2012, 2013; Masilela et al. 2013, Modisha and Nyokong 2014, Masilela et al. 2013 and Mafukidze et al. 2016). This was further demonstrated by their successful application of these fibres in antimicrobial reports in the photodynamic antimicrobial chemotherapy (or PACT) studies (Masilela et al. 2013; Osifeko and Nyokong 2014). An unmodified electrospun fibre (PA alone) was also produced and evaluated for its singlet oxygen-generating ability. In the absence of the Pc sensitizer, the fibre, as expected, did not produce any singlet oxygen.

Photodegradation of Orange G

Spectroscopic characterisation

Figure 6 shows the UV-Vis absorption spectral changes observed upon irradiation of a solution of Orange G at 5-min intervals with the PA/ZnTCPPc-MNP (conj) nanofibre suspended in solution. The absence of the characteristic Q band of the Pc at 680 nm indicates that there is no leaching and the Pc is securely fixed in the nanofibre. The degradation of Orange G was easily monitored by observing the decrease in the dye's absorption band at 478 nm (Deng et al. 2006). Similar UV-Vis absorption spectra were obtained for the PA/ZnTCPPc and PA/ZnTCPPc-MNP (mix) samples. The photolysis of OG involves aryl group hydroxylation, oxidative cleavage of the azo group and desulfonation (Meetani et al. 2011). The oxidative cleavage of the azo group is most likely responsible for the change in solution colour from orange to a colourless solution. The PA/ZnTCPPc-MNP fibre mat, in the absence of irradiation or the phthalocyanine as the sensitizer, showed no significant change in the absorption spectrum of Orange G due to degradation. The latter therefore confirms that the observed photocatalytic activity is due to the ZnTCPPc and that the Pc is embedded in the fibre.

Photodegradation kinetics

The graphs obtained for the variation of the OG concentration versus irradiation time are shown in Fig. 7 for PA/ZnTCPPc-MNP (mix) and the kinetic data obtained is listed in Table 2.

Fig. 6 Absorption spectral changes observed during the photocatalytic degradation of 1.93×10^{-5} mol L^{-1} solution of Orange G using a 15-mg PA/ZnTCPPc-MNP (conj) fibre sample. Irradiation intervals = 10 min

Fig. 7 First-order kinetic plots for the degradation of Orange G carried out at different concentrations: (*i*) 2.3×10^{-5} mol L^{-1}, (*ii*) 3.5×10^{-5} mol L^{-1} and (*iii*) 4.8×10^{-5} mol L^{-1} using the PA/ZnTCPPc-MNP (mix) nanofibre samples
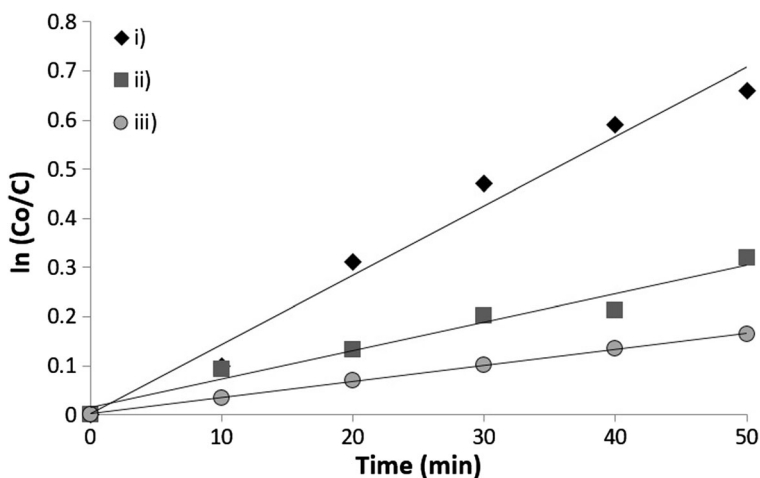
The plots for $\ln(C_o/C)$ versus irradiation time for the PA/ZnTCPPc-MNP (conj) and PA/ZnTCPPc are given in the supplementary information (Fig. S4). These plots give a clearer indication of the degradation of OG for each of the nanofibre samples, and the linearity obtained indicates that the reaction followed first-order kinetics.

The photodegradation rate of Orange G decreased with an increase in OG concentration, with fastest rates observed for the PA/ZnTCPPc-MNP (conj) sample at low OG concentrations. The presence of the MNPs appeared to boost the photodegradation rate of OG as induced by the sensitizer for both the conjugate and mixed samples, an observation that may be directly correlated to the enhancement in singlet oxygen generation observed. Table 2 also reveals reduced half-lives for the OG oxidation on the ZnTCPPc-MNP nanofibre samples as compared to the ZnTCPPc fibre alone,

implying that the effect is due to the presence (either as a conjugate or a mixture) of the MNPs since the singlet oxygen quantum yields improved upon incorporation of the MNPs. Interestingly, the photodegradation rates of the sensitizer or sensitizer hybrids embedded in nanofibres are faster than that for the ZnTCPPc alone or ZnTCPPc-MNP (conj) samples, though this may be due to the differing amounts of Pc present in solution and in the fibre. The half-lives, on the other hand, are shorter for the embedded Pc or Pc conjugates or mixtures (Ledwaba et al. 2015), although the quantities of the photocatalyst employed in these studies may again be different. These data imply that overall the photocatalytic degradation process for OG is more efficient when ZnTCPPc is embedded in a nanofibre. Similar results were obtained by Modisha and Nyokong (2014), where the presence of Fe_3O_4 NPs to enhanced the

Table 2 The initial rate, rate constant (k_{obs}) and half-life ($t_{1/2}$) of the various initial concentrations of Orange G using the functionalised electrospun fibres

Catalyst	[OG] ($\times 10^{-5}$ mol L^{-1})	k_{obs}	Initial rate ($\times 10^{-7}$ mol L^{-1} min^{-1})	Half-life (min)	R^2
PA/ZnTCPPc	2.3	0.050 (0.008)	11.5 (1.8)*	14 (87)	0.984
	3.5	0.006 (0.006)	2.1 (2.0)*	116 (119)	0.882
	4.8	0.002 (0.001)	1.0 (0.5)*	347 (693)	0.780
PA/ZnTCPPc-MNP (conj)	2.3	0.028 (0.030)	6.4 (6.9)*	25 (25)	0.969
	3.5	0.016 (0.010)	5.6 (3.5)*	43 (69)	0.877
	4.8	0.004 (0.002)	1.9 (1.0)*	173 (347)	0.977
PA/ZnTCPPc-MNP (mix)	2.3	0.014	3.2	50	0.979
	3.5	0.006	2.1	116	0.963
	4.8	0.003	1.4	231	0.999

The values in brackets* were obtained for the sample sensitizer samples *not* embedded in the nanofibres (Ledwaba et al. 2015)

photocatalytic ability of the phthalocyanine both upon embedding in a nanofibre and in solution.

Conclusions

The conjugates of ZnTCPPc with gadolinium oxide nanoparticles (MNPs) were successfully incorporated into electrospun nanofibres using the polymer PA-6 (B32 grade). The polymer PA-6 B32 was chosen for further study due to the superior quality of the electrospun nanofibres obtained, as well as the fact that the polyamide polymer is well known for its resistance to heat, durability and strength, making it ideal for filtration purposes. The singlet oxygen-generating ability of the functionalised fibres, as determined by use of the singlet oxygen quencher ADMA, indicated that the functionality of the ZnTCPPc and the ZnTCPPc-MNPs remained intact within a solid fibre core since decent singlet oxygen quantum yields were obtained. The fibres were used to degrade the common water pollutant Orange G, with the highest rates (k_{obs}) achieved by the PA/ZnTCPPc-MNP (conj) fibres. Pseudo-first-order kinetics were followed in the photodegradation of OG for all three functionalised nanofibres. This study has shown that these functionalised mats may be used for water purification purposes, in filtration (due to the presence of the pores in the nanofibre mats) and photo-catalytic applications.

Compliance with ethical standards

Conflict of interest   The authors declare that they have no conflict of interest.

References

Achadu OJ, Uddin I, Nyokong T (2016) Fluorescence behavior of nanoconjugates of graphene quantum dots and zinc phthalocyanines. J Photochem Photobiol A Chem 317:12–25

Agboola B, Ozoemena KI, Nyokong T (2006) Synthesis and electrochemical characterisation of benzyl mercapto and dodecylmercapto tetra substituted cobalt, iron, and zinc phthalocyanines complexes. Electrochemica Acta 51:4379–4387

Ali H, van Lier JE (1999) Metal complexes as photo- and radiosensitizers. Chem Rev 99:2379–2450

Aplin R, Wait TD (2000) Comparison of three advanced oxidation. Processes for Degradation of Textile Dyes Water Sci Technol 42:345–354

Bin Na H, Chan Song I, Hyeon T (2009) Inorganic nanoparticles for MRI contrast agents. Adv Mater 21:2133–2148

Chomoucka J, Drbohlavova J, Huska D, Adam V, Kizek R, Hubalek J (2010) Magnetic nanoparticles and targeted drug delivering. Pharmacol Res 62:144–149

Deng YH, Wang CC, Hu JH, Yang YL, Fu SK (2005) Investigation of formation of silica-coated magnetite nano-particles via sol–gel approach. Colloids Surf A:Physicochem Eng Aspects 62:87–93

Deng J, Jiang J, Zhang Y, Lin X, Du C, Xiong Y (2008)(2006) FeVO$_4$ as a highly active heterogeneous Fenton-like catalyst towards the degradation of Orange II. Appl Catal B 84:468–473

Elliott DW, Zhang WX (2001) Field assessment of nanoscale bimetallic particles for groundwater treatment. Environ Sci Technol 35:4922–4926

Foote CS (1979) In: Wasserman HH, Murray RW (eds) Quenching of singlet oxygen. Academic Press, New York, San Francisco, London, pp 139–171

Goethals A, Mugadza T, Arslanoglu Y, Zugle R, Antunes E, Van Hulle SWH, Nyokong T, De Clerck K (2014) Polyamide nanofiber membranes functionalized with zinc phthalocyanines. J Appl Polym Sci 2014:40486 (7 pages)

Idowu M, Nyokong T (2008) Photosensitizing properties of octacarboxy metallophthalocyanines in aqueous medium and their interaction with bovine serum albumin. J Photochem Photobiol A Chem 200:396–401

Idowu M, Nyokong T (2012) Photophysical behavior of fluorescent nanocomposites of phthalocyanine linked to quantum dots and magnetic nanoparticles. Int J Nanosci 11(2012). Article number 1250018

Kadish K, Smith KM, Guilard R (eds) (2003) Porphyrins handbook: applications of phthalocyanines, vol 19. Academic Press, New York

Lang K, Mosinger J, Kubat P (2016) Nanofibers and nanocomposite films for singlet oxygen based applications. In: Nonell S, Flors C (eds) Singlet oxygen: applications in biosciences and nanosciences, vol 1. Royal Society of Chemistry, Thomas Graham House, Cambridge, pp 305–322. ISBN 978-1-78262-038-9

Ledwaba M, Masilela N, Nyokong T, Antunes E (2015) Surface modification of silica-coated gadolinium oxide nanoparticles with zinc tetracarboxyphenoxy phthalocyanine for the photodegradation of Orange G. J. Mol. Cat. A: Chem. 403: 64–76

Li Y, Pritchett TM, Huang J, Ke M, Shao P, Sun W (2008) Photophysics and nonlinear absorption of peripheral substituted zinc phthalocyanines. J Phys Chem A 112: 7200–7207

Mafukidze DM, Mashazi P, Nyokong T (2016) Synthesis and singlet oxygen production by a phthalocyanine when

embedded in asymmetric polymer membranes. Polymer 105: 203–213

Marais E, Klein R, Antunes E, Nyokong T (2007) Photocatalysis of 4-nitrophenol using zinc phthalocyanine complexes. J Mol Catal A: Chem 261:36–42

Masilela N, Kleyi P, Tshentu Z, Priniotakis G, Westbroek P, Nyokong T (2013) Photodynamic inactivation of *Staphylococcus aureus* using low symmetrically substituted phthalocyanines supported on a polystyrene polymer fiber. Dyes Pigments 96:500–508

Meetani MA, Rauf MA, Hisaindee S, Khaleel A, AlZamly A, Ahmad A (2011) Mechanistic studies of photoinduced degradation of Orange G using LC/MS. RSC Adv 1:490–497

Modisha P, Nyokong T (2014) Fabrication of phthalocyanine-magnetic nanoparticles hybrid nanofibers for degradation of Orange-G. J Mol Cat A: Chem 381:132–137

Modisha P, Antunes E, Mack J, Nyokong T (2013a) Improvement of the photophysical parameters of zinc octacarboxy phthalocyanine upon conjugation to magnetic nanoparticles. Int J Nanosci 12(2013):1350010 10 pp

Modisha P, Nyokong T, Antunes E (2013b) Photodegradation of Orange-G using zinc octacarboxyphthalocyanine supported on Fe_3O_4 nanoparticles. J Mol Cat A: Chem 380:131–138

Mornet S, Vasseur S, Grasset F, Verveka P, Goglio G, Demourgues A, Portier J, Pollert E, Duguet E (2006) Magnetic nanoparticle design for medical applications. Prog Solid State Chem 34:237–247

Mosinger J, Lang K, Kubát P, Sýkora J, Hof M, Plistil L, Mosinger B Jr (2009) Photofunctional polyurethane nanofabrics doped by zinc tetraphenylporphyrin and zinc phthalocyanine photosensitizers. J Fluoresc 19:705–713

Neppolian N, Choi HC, Sakhivel S, Banunathi A, Murugaan V (2002) Solar light induced and TiO_2 assisted degradation of textile dye reactive blue 4. Chemosphere 46:1173–1181

Nyokong T (2006) In: Zagal JH, Bedioui F, Dodelet JP (eds) N4-macrocyclic metal complexes: electrocatalysis, electrophotochemistry, and biomimetric electro-catalysis. Springer, Berlin Chapter 7

Ogunsipe A, Nyokong T (2005) Photophysical and photochemical studies of sulphonated non-transition metal phthalocyanines in aqueous and non-aqueous media. J Photochem Photobiol A Chem 173:211–220

Okura I (2001) Photosensitization of porphyrins and phthalocyanines. Gordon and Breach Publishers, Berlin

Oluwole DO, Tilbury CM, Prinsloo E, Limson J, Nyokong T (2016) Photophysicochemical properties and in vitro cytotoxicity of zinc tetracarboxyphenoxy phthalocyanine—quantum dot nanocomposites. Polyhedron 106:92–100

Osifeko OL, Nyokong T (2014) Applications of lead phthalocyanines embedded in electrospun fibers for the photoinactivation of *Escherichia coli* in water. Dyes Pigments 111(2014):8–15

Rosenthal I, Ben Hur E (1996) In: Leznoff CC, Lever ABP (eds) Phthalocyanines: properties and applications, vol 1–4. Wiley VCH, New York

Spiller W, Kliesch H, Wöhrle D, Hackbarth S, Röder B, Schnurpfeil GJ (1998) Singlet oxygen quantum yields of different photosensitizers in polar solvents and micellar solutions. J Porphyrins Phthalocyanines 2:145–158

Stylidi M, Kondarides DI, Verykios XE (2004) Visible light-induced photocatalytic degradation of Acid Orange 7 in aqueous TiO_2 suspensions. Appl Catal 47:189–201

Sun J, Wang X, Sun J, Sun R, Sun S, Qiao L (2006) Photocatalytic degradation and kinetics of Orange G using nano-sized $Sn(IV)/TiO_2/AC$ photocatalyst. J Mol Catal A Chem 260: 241–245

Tombe S, Chidawanyika W, Antunes E, Priniotakis G, Westbroek P, Nyokong T (2012) Physicochemical behavior of zinc tetrakis (benzylmercapto) phthalocyanine when used to functionalize gold nanoparticles and in electrospun fibers. J Photochem Photobiol A Chem 240:50–58

Tombe S, Antunes E, Nyokong T (2013) Electrospun fibers functionalized with phthalocyanine-gold nanoparticle conjugates for photocatalytic applications. J Mol Catal A Chem 371: 125–134

Wöhrle D, Suvorova O, Gerdes R, Bartels O, Lapok L, Baziakina N, Makarov S, Slodek A (2004) Efficient oxidations and photooxidations with molecular oxygen using metal phthalocyanines as catalysts and photocatalysts. J Porphyrins Phthalocyanines 8:1020–1041

Zhou L, Gu Z, Liu X, Yin W, Tian G, Yan L, Jin S, Ren W, Xing G, Li W, Chang X, Huc Z, Zhao Y (2012) Size-tunable synthesis of lanthanide-doped Gd_2O_3 nanoparticles and their applications for optical and magnetic resonance imaging. J Mater Chem 22:966–974

Zugle R, Litwinski C, Torto N, Nyokong T (2011) Photophysical and photochemical behavior of electrospun fibers of a polyurethane polymer chemically linked to lutetium carboxyphenoxy phthalocyanine. New J Chem 35:1588–1595

Zugle R, Antunes E, Khene S, Nyokong T (2012) Photooxidation of 4-chlorophenol sensitized by lutetium tetraphenoxy phthalocyanine anchored on electrospun polystyrene polymer fiber. Polyhedron 33:74–81